

Article

Numerical Investigation on Flow Characteristics and Aerodynamic Performance of a 1.5-Stage SCO_2 Axial-Inflow Turbine with Labyrinth Seals

Qiuwan Du and Di Zhang * 

MOE Key Laboratory of Thermo-Fluid Science and Engineering, School of Energy and Power Engineering, Xi'an Jiaotong University, Xi'an 710049, China; duqiuwan@stu.xjtu.edu.cn

* Correspondence: zhang_di@mail.xjtu.edu.cn; Tel.: +86-029-8266-6559

Received: 1 December 2019; Accepted: 27 December 2019; Published: 3 January 2020



Abstract: The leakage problem of supercritical carbon dioxide (SCO_2) axial-inflow turbine brings great challenges to the efficiency and security of the power system. Labyrinth seals are usually utilized to improve the leakage characteristics of the blade tip. In this paper, a 1.5-stage SCO_2 axial-inflow turbine is established and labyrinth seals are arranged on the top of the first stage stator and rotor blades. The effects of seal clearance, groove on seal cavity surface and circle groove shape on flow characteristics and aerodynamic performance under different pressure ratio are investigated. Increasing seal clearance can significantly weaken the turbine performance. Arranging rectangle, circle and V-shaped grooves on the seal cavity surface near the outlet of the seal gap can enhance the energy dissipation, reduce the relative leakage and improve the power and efficiency. Increasing the groove width can improve the aerodynamic performance while the effect of the groove depth is weak. The configuration where the circle groove width is 50% of the pitch of seal tooth achieves the best performance with the relative leakage of stator1 and rotor, power and efficiency of 6.04×10^{-3} , 8.09×10^{-3} , 3.467 MW and 86.86% respectively. With an increase in pressure ratio, the relative leakage increases firstly and then remains almost constant. The power increases while the efficiency increases firstly and then decreases, reaching the peak value under the design condition.

Keywords: supercritical carbon dioxide; axial-inflow turbine; labyrinth seal; flow characteristics; aerodynamic performance

1. Introduction

Supercritical carbon dioxide (SCO_2) has excellent physical properties and can bring outstanding compactness and high efficiency to the Brayton cycle power system [1]. In recent years, the Brayton power cycle system with SCO_2 as working fluid has been widely investigated by scholars [2–5]. The turbine is the core part of the power cycle system, which plays a critical role in generating power. The axial-inflow turbine becomes the best choice when large output power is required. In order to improve the vibration performance, the shrouded blades are usually utilized. The leakage of working fluid at the tip clearance causes a decrease in power and efficiency. Under these circumstances, the labyrinth seal (LS) is generally utilized for the reduction in leakage [6].

A series of research on the performance of LS has been carried out, most of which are focused on the influence of structural parameters. Yahya [7] numerically analyzed the performance of LS considering mushroom wear and explored the effects of seal clearance, pressure ratio, number of teeth and velocity. Zhang [8] investigated the performance of stepped LS under different structural parameters. The difference of leakage mechanism between the upwind and backwind structures has also been obtained. The Computational Fluid Dynamics (CFD) method was adopted to study the

influence of structural and operation parameters on tangential friction coefficients by Wu [9] and the leakage performance of four LS configurations was also studied [10]. Włodzimierz [11] optimized the structural variables of LS with honeycomb holes and achieved a reduction in leakage. Parametric research on a type of LS with honeycomb holes was conducted by Kali [12] and the influence of honeycomb size, pressure ratio and clearance on performance was obtained. Alessio [13] studied the effect of gap thickness on mass flow coefficient under different working conditions. Yan [14] experimentally and numerically investigated the influence of the stator hole on the performance of LS.

However, the above research was only carried out for LS without consideration of the blade region. The coupled analysis of LS and blade was also conducted by plenty of scholars. Giboni [15] studied the mixing effect of flows in leakage passage and cascade when the LS was arranged on the top of the rotor blade. The results agreed utterly with the test data. A new type of radial seal was proposed by Zhang [16], and the large flow resistance and low leakage were achieved compared with the traditional LS. Liu [17] concluded that the LS arranged on the top of the shroud can significantly reduce the total pressure loss. Flow characteristics of LS on an axial-flow turbine were investigated with low Mach number preconditioning technique by Jens [18]. Krzysztof [19] developed a type of cavity seal and greatly reduced the aerodynamic force of LS under small clearance. Zou [20] proposed a multi-dimensional coupling simulation method to study the flow field characteristics of a turbine with LS under various operating conditions. The numerical study carried out by Marc [21] proved that the interaction of flows mainly affects the top flow field.

It is noted that although there is some research on the performance of LS arranged on the top of the blade shroud, the selected working fluid is all air or gas. However, there are major differences between the physical properties of SCO_2 and air, such as density, viscosity and compress factor. It is necessary to investigate the performance of LS with SCO_2 as a working fluid. Only Yuan [22] and Kim [23] have carried out a preliminary investigation on SCO_2 LS, but comprehensive research on SCO_2 LS coupled with a blade is also in absence.

Therefore, the investigation on a SCO_2 axial-inflow turbine with LS is carried out in this paper. Configurations with LS arranged on the top of the shroud of both stator and rotor blade are established. The flow characteristics and aerodynamic performance of configurations with different seal clearance under various working conditions are analyzed. Furthermore, the effect of groove on the cavity surface on the performance is studied and the optimal groove shape is obtained. The work in this paper makes great contributions to further research and application of LS on the top of the shrouded blade of SCO_2 axial-inflow turbine.

2. Numerical Methodology

2.1. Physical Model

The research objective in this paper is selected as a 1.5-stage SCO_2 axial-inflow turbine, which includes stator1, rotor and stator2. The LS is arranged on the top of the shroud of stator1 and rotor. The extended sections are provided at both the inlet and outlet. The schematic diagrams of blades and seal structures are shown in Figures 1 and 2 respectively. The structural parameters of blades and seal structures are listed in Tables 1 and 2 respectively. The design condition parameters are listed in Table 3.

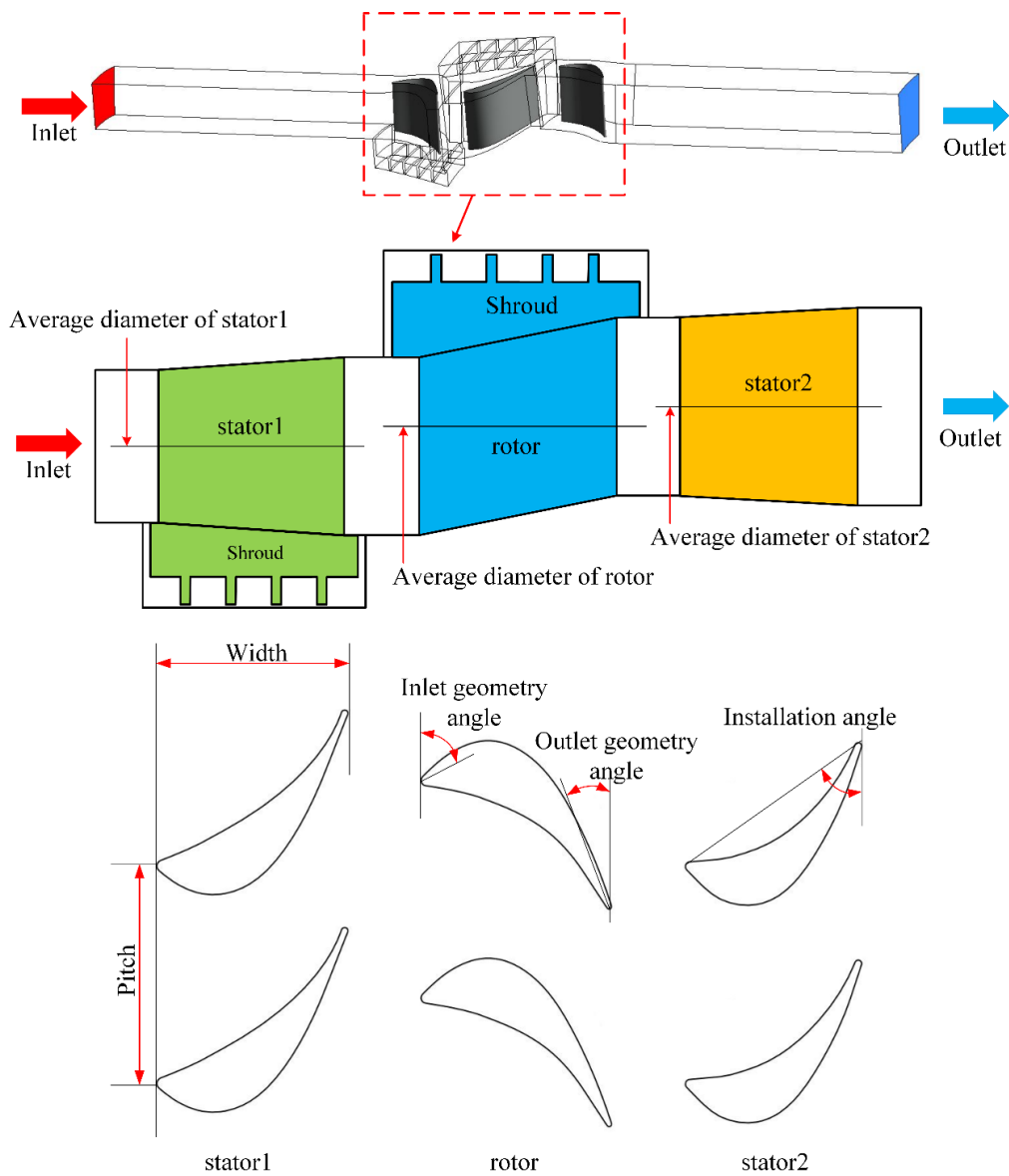


Figure 1. Schematic diagram of the 1.5-stage turbine.

Table 1. The geometry parameters of stator and rotor blades.

| Item | Stator 1 | Rotor | Stator 2 |
|-------------------------|----------|--------|----------|
| Blade number | 28 | 35 | 33 |
| Width/mm | 25 | 25 | 23 |
| Height/mm | 20 | 25 | 23 |
| Pitch/mm | 30 | 22 | 31 |
| Average diameter/mm | 247.52 | 255.60 | 263.68 |
| Installation angle/° | 39 | 55 | 35 |
| Inlet geometry angle/° | 10 | 20 | 20 |
| Outlet geometry angle/° | 70 | 62 | 70 |

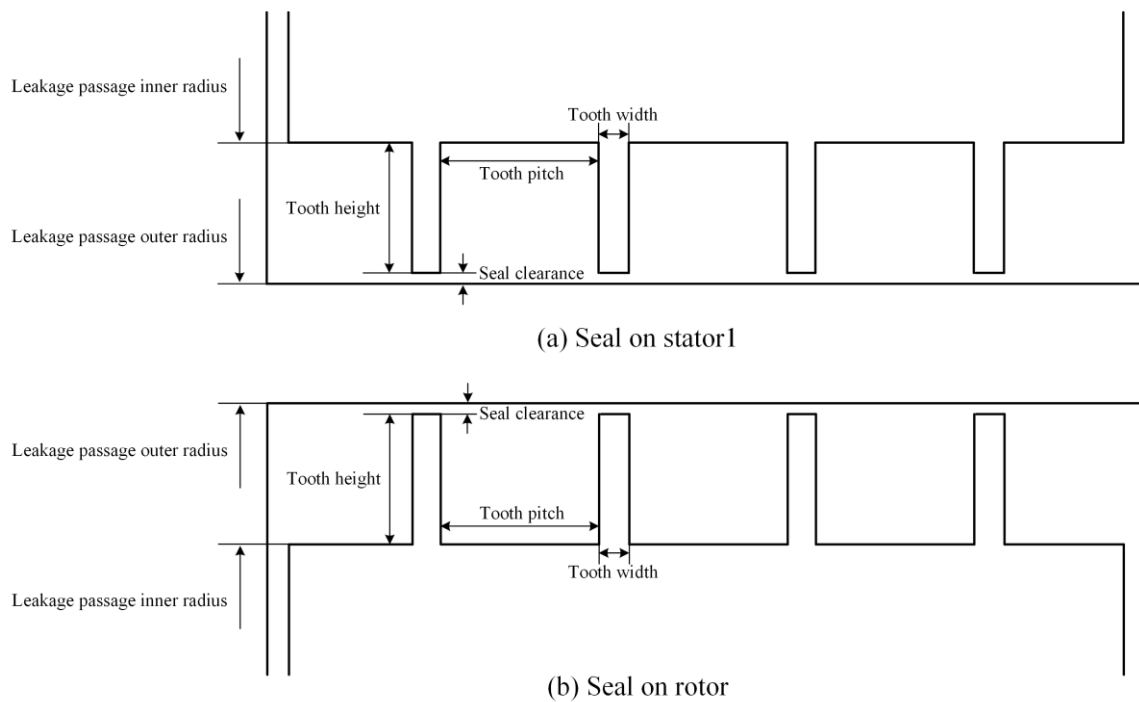


Figure 2. Schematic diagram of the seal structures.

Table 2. Geometry parameters of seal structures.

| LS on Stator1 | | LS on Rotor | |
|---------------------------------|--------|---------------------------------|-------|
| Items | Value | Items | Value |
| Leakage passage outer radius/mm | 106.26 | Leakage passage outer radius/mm | 153.2 |
| Leakage passage inner radius/mm | 101.06 | Leakage passage inner radius/mm | 148 |
| Tooth number | 4 | Tooth number | 4 |
| Tooth height/mm | 5 | Tooth height/mm | 5 |
| Tooth width/mm | 1 | Tooth width/mm | 1 |
| Seal clearance (C)/mm | 0.2 | Seal clearance (C)/mm | 0.2 |
| Tooth pitch (P)/mm | 5.8 | Tooth pitch (P)/mm | 5.8 |

Table 3. The boundary conditions.

| Item | Value |
|----------------------------|--------|
| Inlet total pressure/MPa | 15 |
| inlet total temperature/K | 773.15 |
| outlet static pressure/MPa | 11.09 |
| Rotation speed/rpm | 10,000 |

2.2. Governing Equation

In the analysis of the flow fields, the continuity equation, momentum equation and energy equation can be expressed as the following unified form:

$$\nabla \cdot (\rho u \varphi) = \nabla \cdot (\Gamma \text{grad} \varphi) + S, \tag{1}$$

where φ is the general form of physical variables, Γ is the generalized diffusion coefficient and S is the generalized source term. When they are expressed as the following forms in Equations (2), Equation (1) represents the continuous equation, momentum equation and energy equation respectively.

$$\varphi = \begin{bmatrix} 1 \\ u_i \\ T \end{bmatrix}, \Gamma = \begin{bmatrix} 0 \\ \mu \\ k/C_p \end{bmatrix}, S = \begin{bmatrix} 0 \\ -\text{grad}p \\ 2\mu\nabla \cdot (\text{grad}u)/C_p \end{bmatrix}, \quad (2)$$

where u denotes velocity and subscript i denotes velocity directions. T is the temperature and k is the thermal conductivity. p represents the pressure and C_p represents the specific heat capacity. And μ is the dynamic viscosity coefficient.

2.3. Mesh Strategy and Boundary Conditions

The computational mesh utilized for the numerical simulation is presented in Figure 3. All the domains are meshed by hexahedral structured grid generated by ICEM CFD. The boundary layers are adopted near the wall to ensure calculation accuracy. The first cell size is selected as 2×10^{-4} mm and the y^+ value is less than 1.

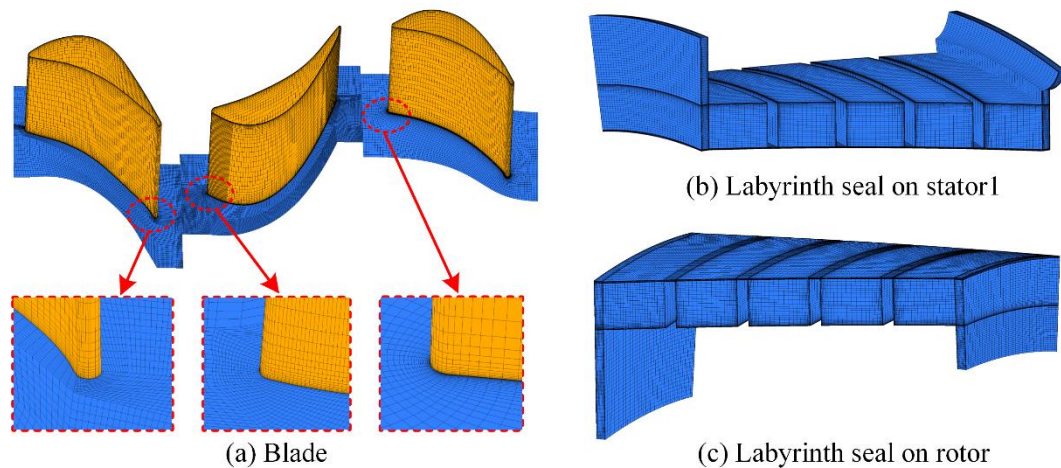


Figure 3. Computational Mesh.

The flow in blade cascade and LS is complex turbulence. In this paper, the commercial software ANSYS CFX18.2 is selected and the Shear Stress Transfer (SST) model is utilized for calculation [20,24,25]. The working fluid is SCO_2 and the accurate physical properties are from NIST [26]. The property data is imported in software by the RGP format file to achieve the accurate simulation.

The boundary conditions are introduced as follows. The periodic symmetric model is adopted for lower calculation cost. The detailed condition parameters are shown in Table 3. The interface is set between the contacted surfaces of two adjacent domains and the other surfaces are set as adiabatic. The frozen rotor method is adopted to deal with rotating and stationary interfaces [24,27,28].

The mass flow rate and output power are two important performance parameters of the axial-inflow turbine. Thus, the grid independence study is carried out for these two parameters. The output power is defined as:

$$W = \frac{2\pi n}{60} \times T_z, \quad (3)$$

where n represents rotation speed and T_z denotes torque of rotor along axial direction.

The seal clearance is selected as 0.2 mm. The grid independence study is conducted base on the mass flow rate and power. It concludes from the results shown in Table 4 that the variations of these two parameters are almost negligible after the grid number exceeds 2.5×10^6 . Therefore, the adopted grid number in this paper is 2.5×10^6 .

Table 4. Grid independence study.

| Grid Number | Mass Flow Rate/(kg/s) | Deviation/% | Power/kW | Deviation/% |
|-------------------|-----------------------|-------------|----------|-------------|
| 5×10^5 | 135.82 | - | 3.373 | |
| 1.2×10^6 | 136.18 | 0.264 | 3.384 | 0.325 |
| 1.8×10^6 | 138.14 | 1.419 | 3.435 | 1.485 |
| 2.5×10^6 | 138.25 | 0.079 | 3.442 | 0.203 |
| 3.2×10^6 | 138.26 | 0.007 | 3.443 | 0.029 |

2.4. Validation

Yuan [22] has carried out numerical and experimental research on the SCO₂ flow in the straight-through LS. In this paper, the same geometric structure as [22] is established and the CFD simulation research is carried out under the same working conditions with the above numerical method. The geometric structure and analysis results are demonstrated in Figure 4. It can be found that the maximum difference reaches 5.69% at the pressure ratio of 0.915, which is within the acceptable range of 10%. Moreover, the better consistency between CFD results in this paper and experimental data in [22] is found compared with the CFD results in [22] under various conditions. Therefore, the simulation accuracy of the numerical method in this paper is fully verified.

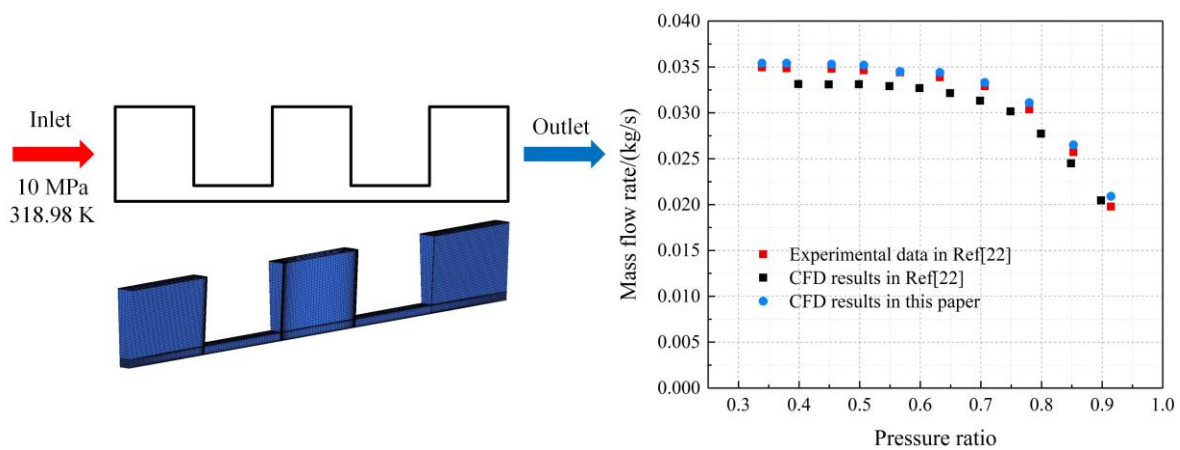


Figure 4. The geometric structure and analysis results for validation.

3. Results and Discussions

3.1. Effect of Seal Clearance

Seal clearance is a critical variable that affects the performance of LS. In this chapter, straight LS teeth are arranged on the top of stator1 and rotor.

The no-dimensional seal clearance is defined by

$$\bar{C} = \frac{C}{H_{in}}, \tag{4}$$

where, H_{in} represents the blade height at inlet of rotor.

The no-dimensional seal clearances (\bar{C}) are 0.004, 0.008, 0.012 and 0.016 respectively. The flow characteristics and aerodynamic performance of four configurations under different speed and pressure ratio are discussed in detail.

The static pressure contours of meridional planes of four configurations under the design condition are demonstrated in Figure 5. In the cascade passage, the pressure decreases gradually along the flow direction. The rotor passage bears the maximum pressure drop due to the fact that the working fluid pushes the rotor blade to generate power. In the top leakage passage of stator1 and rotor, the pressure

also gets reduced along the flow direction. Vortex is formed in the cavity between each LS tooth, which is caused by the throttling and expansion effect at the seal gap. The existence of secondary flow further leads to energy dissipation and pressure drop. Furthermore, the mixing effect generated by the main flow and leakage flow at the outlet of leakage passage is raised gradually with an increase in seal clearance, which is represented by the deflection of nearby main flow streamline and even the local vortex. This has a notable effect on turbine performance.

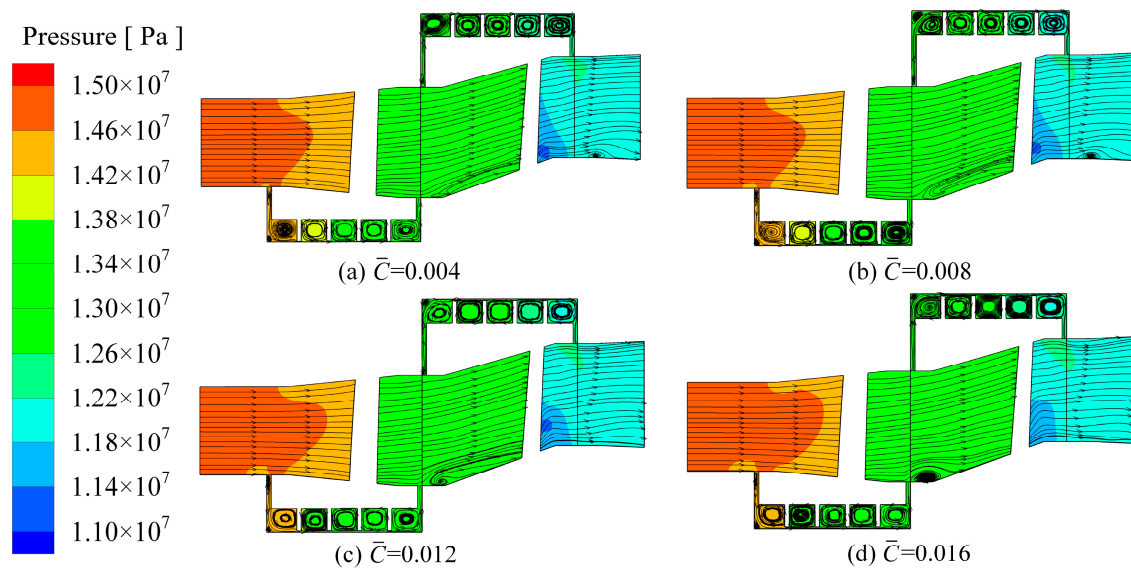


Figure 5. The static pressure contours of the meridional planes.

The static entropy contours of meridional planes of four configurations under the design condition are depicted in Figure 6. It concludes that the static entropy in the main flow passage is always at a low level. High static entropy is observed in the central area of the seal cavity, indicating chaotic flow and high energy loss. The static entropy at the outlet of leakage passage increases gradually with an increase in seal clearance, indicating a gradual increase in energy loss. This is because when the leakage flow enters the cascade, it has a certain radial velocity. This is quite different from the main flow along the axial direction, resulting in a high mixing loss.

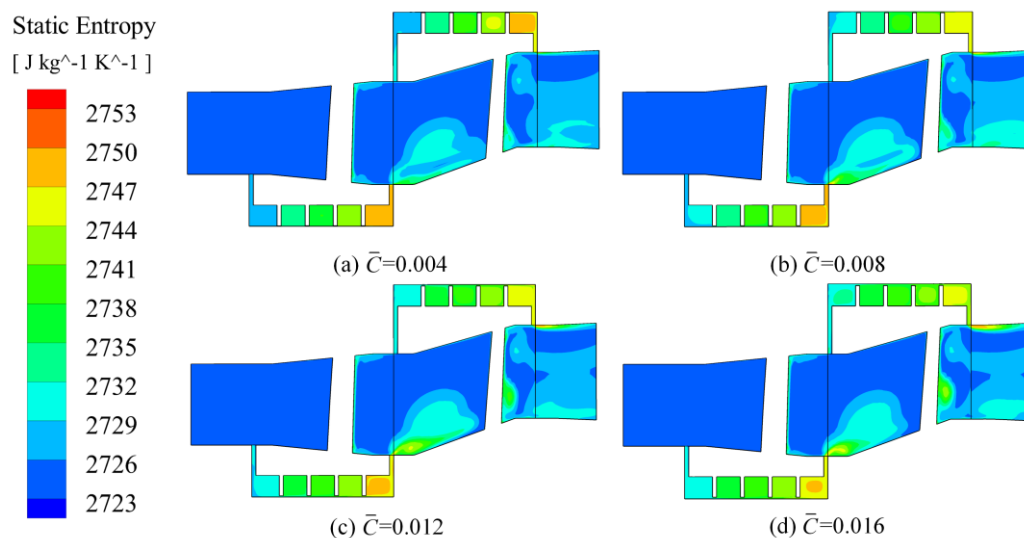


Figure 6. The static entropy contours of the meridional planes.

When the leakage flow of stator1 enters the rotor cascade, it affects the flow field distribution of the rotor near the hub side. Similarly, the flow field distribution of stator2 near the shroud side is affected by the leakage flow of the rotor. Therefore, the flow characteristics of 1% blade height of the rotor and 99% blade height of stator2 are obtained, indicated in Figure 7. It is observed that there is a strong mismatch between the angle at the inlet side and the geometry installation angle because of the mixing of the main flow and leakage flow. Moreover, the stronger mismatch and disordered streamlines are achieved as the seal clearance increases, causing the reduction of the working ability of the rotor blade.

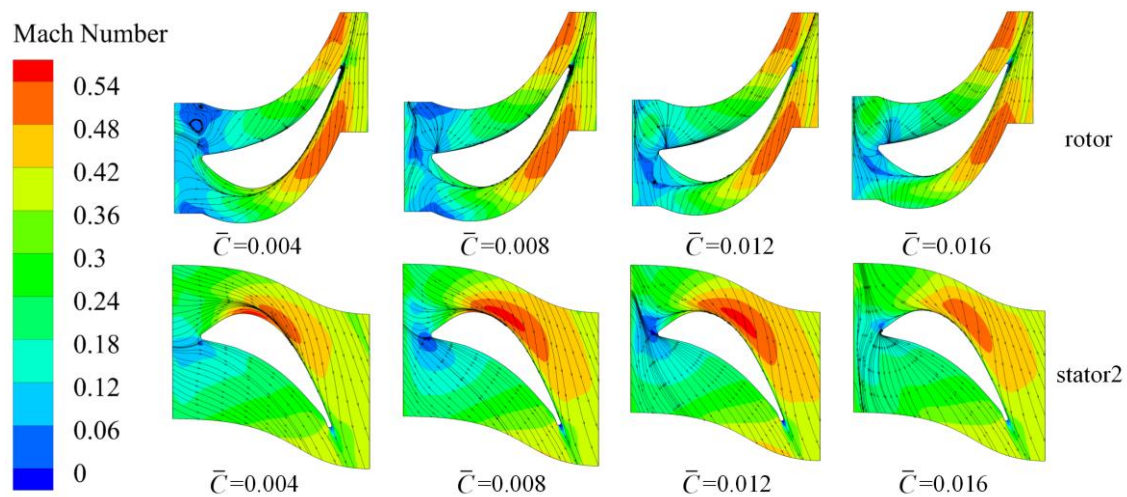


Figure 7. The Mach number contours: (up: 1% blade height of rotor; down: 99% blade height of stator2).

In order to further analyze the static pressure distribution of blade surface considering the leakage flow, the static pressure distributions of four configurations under the design condition are depicted in Figure 8. For the 1% blade height of the rotor, the pressure on the suction side from the leading edge to the 70% chord length increases gradually as the seal clearance increases. This results in the reduction of the pressure difference between the pressure side and suction side, further causing the reduction of the power capacity of the rotor blade. For the 99% blade height of stator2, the increase of seal clearance leads to the raising of pressure on the suction side from the leading edge to 90% chord length. Especially when \bar{C} is 0.016, the cross of pressure distribution curves at the leading edge of stator2 indicates the existence of a negative attack angle, serious streamline deflection and further terrible aerodynamic performance.

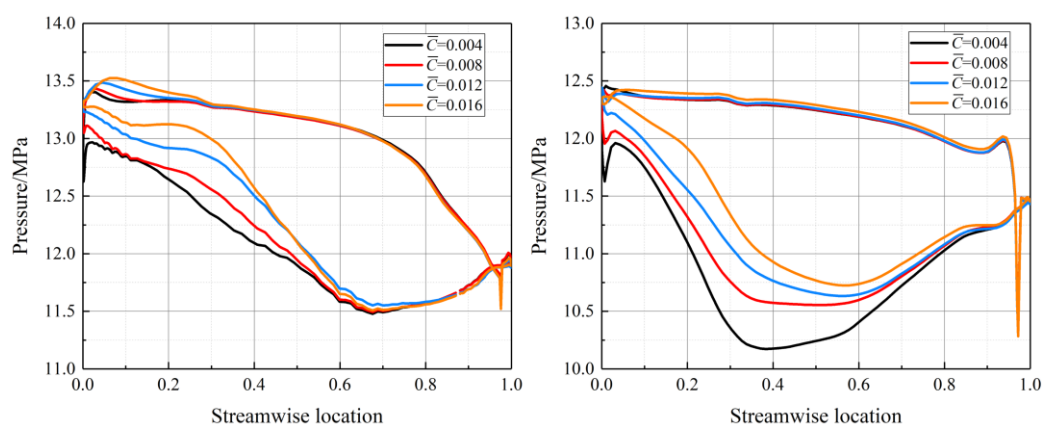


Figure 8. The static pressure distributions under different seal clearance: (left: 1% blade height of rotor; right: 99% blade height of stator2).

For the sake of more detailed analysis on the turbine performance, the following performance parameters are defined.

The isentropic efficiency is given by

$$\eta = \frac{W}{\Delta h_{is} \cdot \dot{m}}, \tag{5}$$

Relative leakage of LS on stator1 is defined by

$$L_s = \frac{\dot{m}_{sout}}{\dot{m}}, \tag{6}$$

Relative leakage of LS on rotor is defined by

$$L_r = \frac{\dot{m}_{rout}}{\dot{m}}, \tag{7}$$

where Δh_{is} represents the isentropic enthalpy drop from the inlet of stator1 to the outlet of stator2. \dot{m} represents the mass flow rate. \dot{m}_{sout} and \dot{m}_{rout} denote the mass flow rate at the outlet of the leakage passage on stator1 and rotor respectively.

The variations of relative leakage, power and efficiency with pressure ratio are presented in Figure 9. Under any working condition, the relative leakage of stator1 and rotor increase while the power and efficiency decrease with an increase in seal clearance. Below the design condition point, the relative leakage increases sharply with an increase in seal clearance. However, the leakage is almost kept constant after the pressure ratio exceeds the design pressure ratio. The efficiency increases firstly and then decreases. This is because there is the optimal speed ratio near the design point. When the speed ratio deviates from the design point, the residual speed loss increases, causing a reduction of efficiency. The power increases gradually as the pressure ratio increases, which is mainly due to the raising of the mass flow rate and enthalpy drop. Furthermore, the relative leakage of the rotor is always higher than that of stator1. This can be explained by the fact that pressure drop from the inlet to the outlet of the rotor is the largest because the working fluid pushes the rotor blade to generate power.

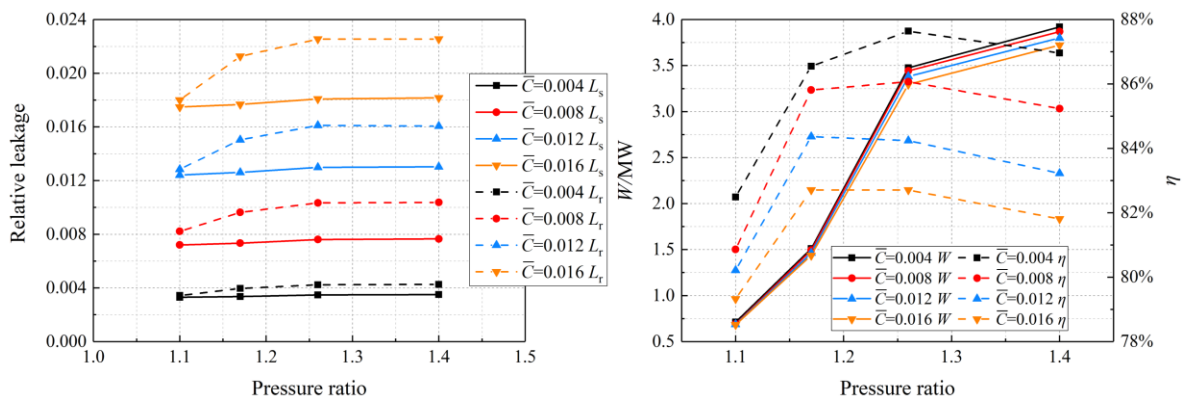


Figure 9. Variations of performance parameters under different seal clearance with pressure ratio (left: relative leakage; right: power and efficiency).

3.2. Effect of Groove on Cavity Surface

The energy dissipation and sealing performance are achieved by throttling and expansion effect at the seal gap and vortex formed in the seal cavity. The change of the seal cavity wall shape affects the secondary flow and further the energy dissipation in the seal cavity. Therefore, three types of grooves, namely rectangle, circle and V-shaped, are set on the cavity wall near the seal gap outlet. The influence of the groove on the flow characteristics and aerodynamic performance is investigated.

The non-dimensional groove depth is given by

$$\bar{D} = \frac{D}{C}, \tag{8}$$

The non-dimensional groove width is given by

$$\bar{H} = \frac{H}{P}, \tag{9}$$

where D denotes groove depth and H denotes groove width.

The profiles of the three types of structures are illustrated in Figure 10. Where, according to the geometric structure, the values of \bar{C} , \bar{D} and \bar{H} are set as 0.008, 3.5 and 0.3 respectively.

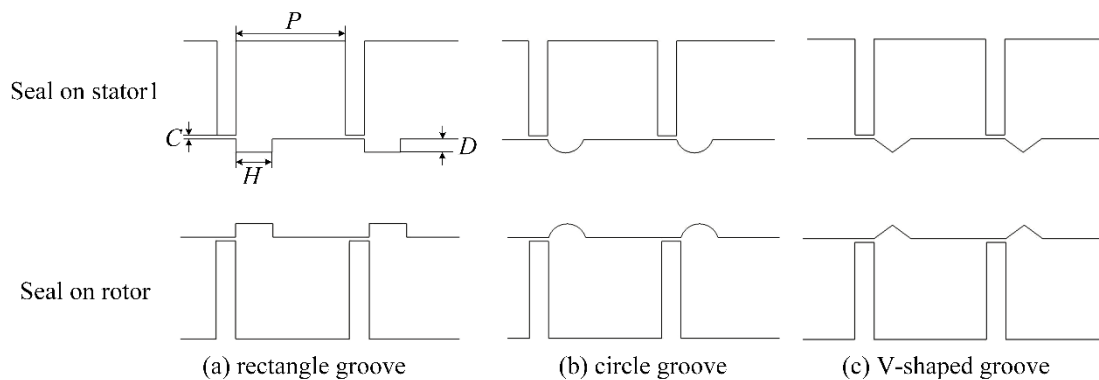


Figure 10. Profiles of seals under different cavity surface shape.

The Mach number contours of the meridional plane of leakage passage on stator1 and rotor of different structures are presented in Figures 11 and 12 respectively. The flow field distribution of the two leakage passages is similar. After the working fluid flows through the seal gap, a large vortex is formed in the seal cavity and a small one with reverse direction is produced in both rectangle and circle groove. This further strengthens the disturbance of the working fluid and enhances the energy dissipation. However, for the V-shaped groove, only a tiny vortex is generated at the bottom of the groove, and most streamlines are only slightly deflected.

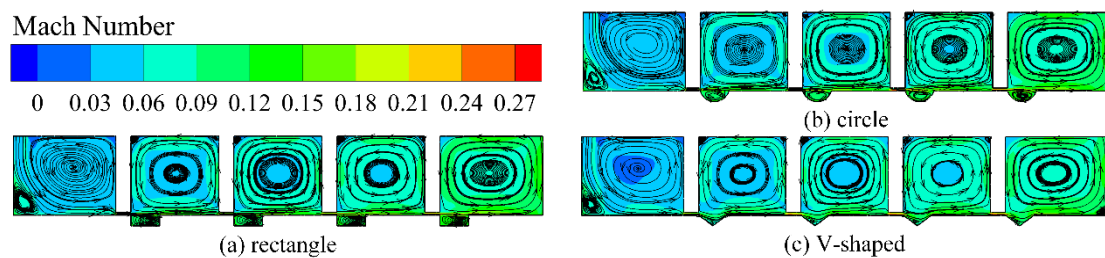


Figure 11. The Mach number contours of meridional plane of leakage passage on stator1.

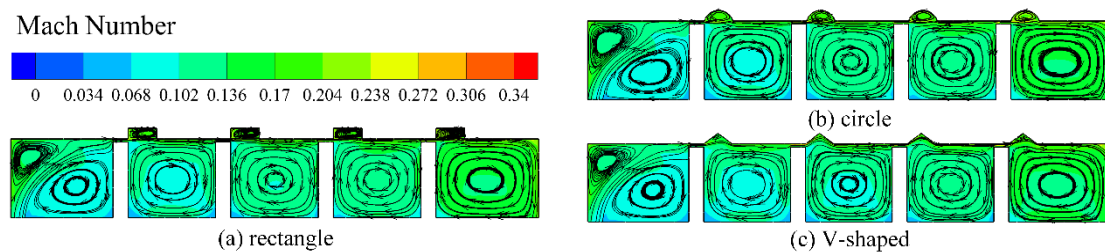


Figure 12. The Mach number contours of meridional plane of leakage passage on rotor.

The pressure distributions in Line1 and Line2 are selected to characterize the pressure distributions in leakage passages along an axial direction, just as shown in Figure 13. Where Line1 is the intersection line of the X–Z plane and the outer surface of leakage passage on stator1. Line2 is the intersection line of the X–Z plane and the outer surface of leakage passage on rotor1. The pressure drop along the flow direction can be observed clearly. Due to the throttling effect at the inlet of the seal gap, the flow acceleration occurs and the pressure decreases significantly. Moreover, a local expansion exists at the outlet of the seal gap and the local pressure increased. The pressure in the seal cavity with groove is much higher than that in the seal cavity without groove, which is the conversion of more kinetic energy to potential energy owing to the enhanced flow disturbance.

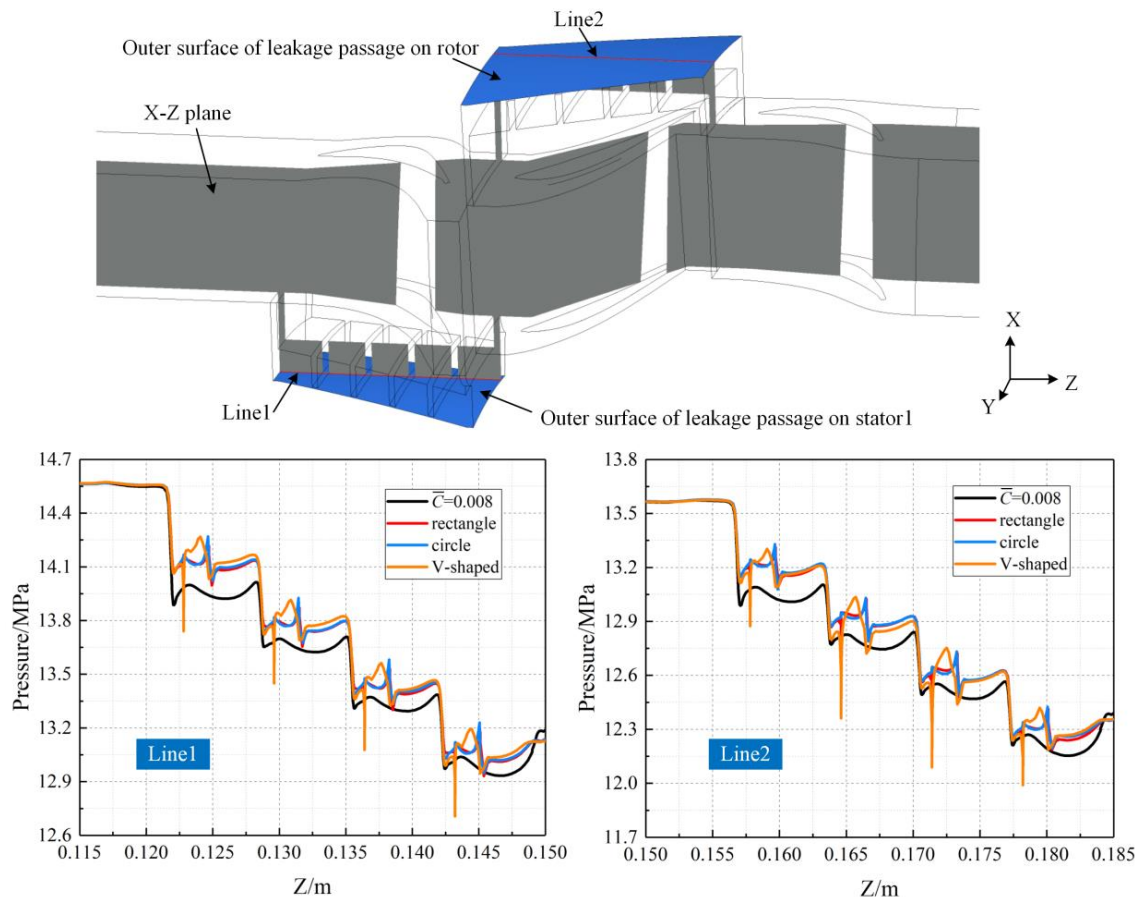


Figure 13. The distributions of pressure in leakage passage along axial direction under different groove on the cavity surface.

The variations of relative leakage, power and efficiency under different groove on the cavity surface with pressure ratio are presented in Figure 14. Configurations with groove have lower leakage, higher power and efficiency compared with the non-grooved configuration under any working condition. It can conclude that arranging groove on the seal cavity wall near the outlet of the seal gap can enhance the sealing effect and improve the aerodynamic performance. Further comparison shows that the configuration with circle groove achieves the lowest leakage, the highest power and efficiency. This can be explained by the following fact. From the streamline distributions in Figures 11 and 12, it can be seen that no vortex is formed in the V-shaped groove and most streamlines are only slightly deflected. Thus, the energy dissipation in the leakage channel is the lowest and the performance is relatively the worst. As for the rectangle and circle groove, there are local small vortices which are opposite to the large vortices in the seal cavity. The interaction between these reverse vortices enhances the energy dissipation and leads to better performance. Furthermore, the better matching degree between the

circle groove profile and the outline of the local small vortex for circle groove is observed. The energy dissipation caused by the small vortex near the stationary surface of the circle groove is higher than that of the rectangle groove. Therefore, the circle groove achieves the best performance. Under the design condition, the relative leakage of stator1 and rotor, power and efficiency are 6.34×10^{-3} , 8.53×10^{-3} , 3.463 MW and 86.61% respectively. With an increase in pressure ratio, the variation trends of these four parameters are the same as those in Section 3.1. Below the design point, the relative leakage increases rapidly with an increase in pressure ratio. After the pressure ratio exceeds the design value, the relative leakage is almost unchanged. As the pressure ratio increases, the power increases while the efficiency increases firstly and then decreases.

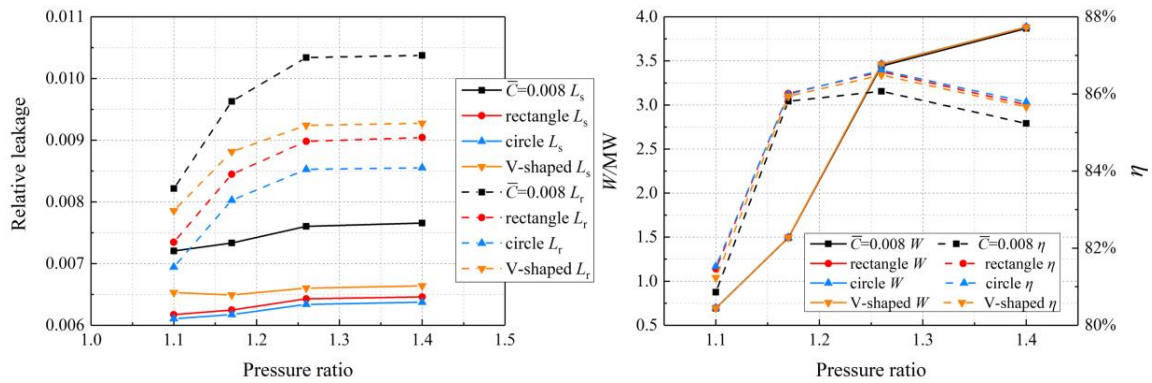


Figure 14. Variations of performance parameters under different groove on cavity surface with pressure ratio (left: relative leakage; right: power and efficiency).

3.3. Effect of Circle Groove Shape

It concludes through the above analysis that the configuration with circle groove achieves the most outstanding performance. Configurations with circle groove under different width and depth are established to study the effect of circle groove shape on flow characteristics and aerodynamic performance in this chapter. Specifically, five types of configurations are established by changing W and D . The structural parameters of five cases are shown in Table 5. Where case1 is the configuration with circle groove established in Section 3.2. The schematic diagram of the five cases is illustrated in Figure 15.

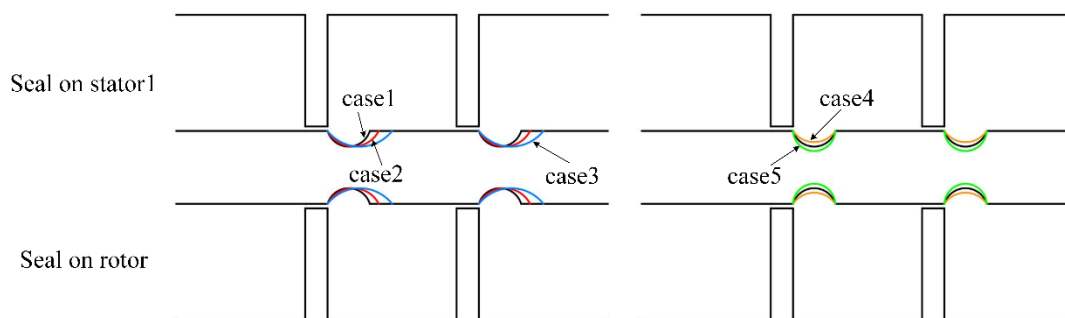


Figure 15. Profiles of five cases.

The Mach number contours of the meridional plane of leakage passage on stator1 and rotor of five cases are depicted in Figures 16 and 17 respectively. By comparing case1, case2 and case3, with an increase in groove width, the vortex is formed in the front half of the circle groove in the opposite direction to that in the seal cavity. The streamlines in the back half deflect, and the working fluid flows into the seal cavity after impacting the groove bottom. By the comparison of case1, case4 and case5, the flow field distribution trends in the circle groove are almost the same. With an increase in groove depth, the size of the vortex is raised.

Table 5. Configurations of circle grooves.

| Case | W/mm | P/mm | D/mm | C/mm | \bar{C} | \bar{D} | \bar{H} |
|------|------|------|------|------|-----------|-----------|-----------|
| 1 | 1.74 | 5.8 | 0.7 | 0.2 | 0.008 | 3.5 | 0.3 |
| 2 | 2.32 | 5.8 | 0.7 | 0.2 | 0.008 | 3.5 | 0.4 |
| 3 | 2.9 | 5.8 | 0.7 | 0.2 | 0.008 | 3.5 | 0.5 |
| 4 | 1.74 | 5.8 | 0.5 | 0.2 | 0.008 | 2.5 | 0.3 |
| 5 | 1.74 | 5.8 | 0.9 | 0.2 | 0.008 | 4.5 | 0.3 |

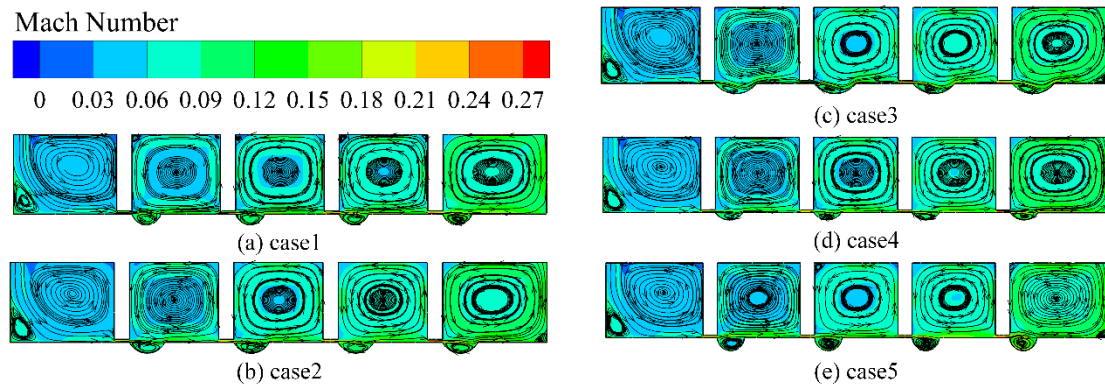


Figure 16. The Mach number contours of meridional plane of leakage passage on stator1 of case1–5.

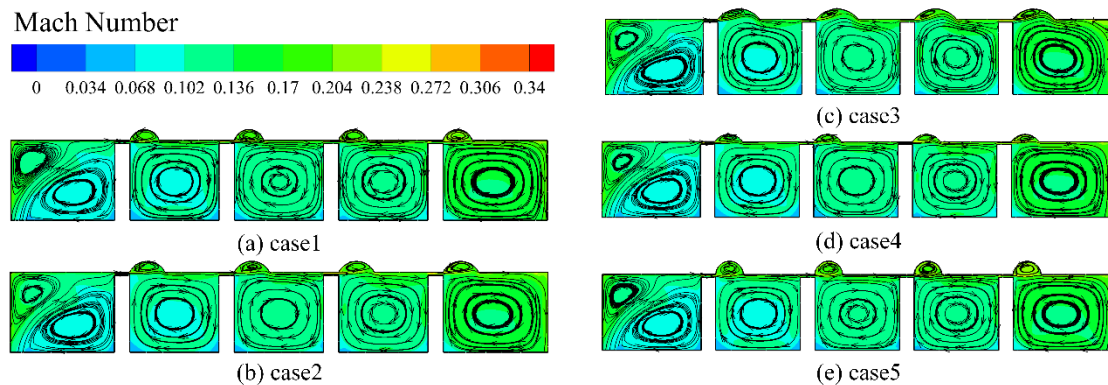


Figure 17. The Mach number contours of meridional plane of leakage passage on rotor of case1–5.

Similar to the above chapter, the pressure distributions in Line1 and Line2 are presented in Figure 18. The distribution trends are similar to that in Section 3.2. The pressure decreases gradually along the flow direction in general. There is a local pressure drop at the inlet of the seal gap and local pressure rises at the outlet of the seal gap respectively. The detailed comparison suggests that the variation of width changes the axial position of the pressure rise in the circle groove while the variation of depth affects the peak value of the pressure in the circle groove.

The variations of relative leakage, power and efficiency of five cases with pressure ratio are presented in Figure 19. By comparing case1, case2 and case3, case3 holds the lowest leakage, the highest power and efficiency. The relative leakage of stator1 and rotor, power and efficiency under the design condition are 6.04×10^{-3} , 8.09×10^{-3} , 3.467 MW and 86.86% respectively. It proves that increasing groove width can improve aerodynamic performance. In addition, these performance parameters of case1, case4 and case5 are very close with a tiny difference. It concludes that the groove depth has little impact on aerodynamic performance. The variation trends of these performance parameters with pressure ratio are the same as those in Sections 3.1 and 3.2. The relative leakage gets increased as the pressure ratio is raised to the design value. The influence of the pressure ratio on the relative leakage is

weak when it exceeds the design value. The power increases while the efficiency increases first and then decreases as the pressure ratio increases.

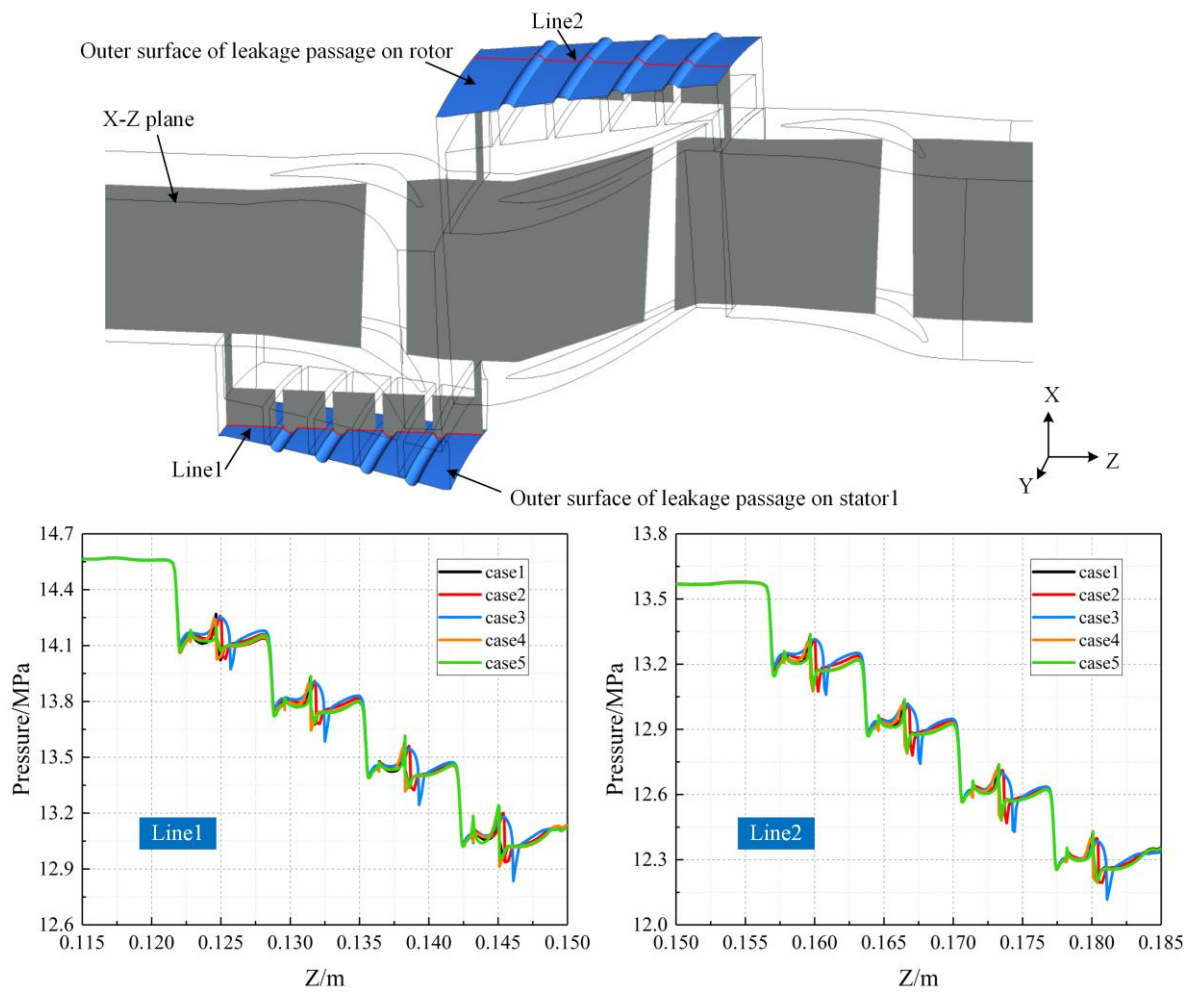


Figure 18. The distributions of pressure in leakage passage along axial direction of case1–5.

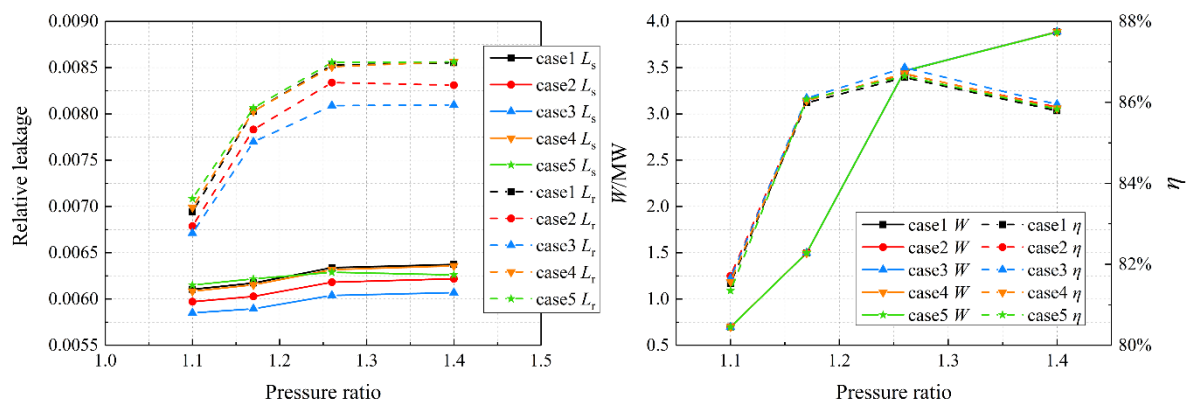


Figure 19. Variations of performance parameters of case1–5 with pressure ratio (left: relative leakage; right: power and efficiency).

4. Conclusions

In this paper, a 1.5-stage SCO_2 axial-inflow turbine with LS on the top of the first stage stator and rotor blades are established. The flow characteristics and aerodynamic performance under different

seal clearance are investigated. Furthermore, the rectangle, circle and V-shaped grooves are arranged on the seal cavity surface. The investigations on the performance of these three configurations under various working conditions are studied. Finally, the effect of the circle groove shape is discussed in detail. Specifically, the following conclusions are drawn.

- (1) Seal clearance has a significant influence on turbine performance. With an increase in seal clearance, the mixing of the main flow and leakage flow gets stronger and the loss gets larger. Furthermore, the relative leakage increases while the power and efficiency decrease.
- (2) Arranging rectangle, circle and V-shaped grooves on the seal cavity surface near the outlet of the seal gap can enhance the energy dissipation, reduce the relative leakage and improve the power and efficiency. Moreover, the configuration with the circle groove performs the best. The relative leakage of stator1 and rotor, power and efficiency under the design condition are 6.34×10^{-3} , 8.53×10^{-3} , 3.463 MW and 86.61% respectively.
- (3) For the geometric parameters in this paper, increasing the circle groove width can improve the aerodynamic performance. However, the groove depth has little effect on performance. The configuration where the groove width is 50% of the pitch of seal tooth achieves the best performance. The relative leakage of stator1 and rotor, power and efficiency under the design condition are 6.04×10^{-3} , 8.09×10^{-3} , 3.467 MW and 86.86% respectively.
- (4) Under the same working condition and structural parameters, the relative leakage of the rotor is always higher than that of stator1. With an increase in pressure ratio, the relative leakage increases firstly and then remains unchanged. The power increases while the efficiency increases firstly and then decreases, reaching the peak value under the design condition.

Author Contributions: Conceptualization, Q.D. and D.Z.; methodology, Q.D.; software, Q.D.; validation, Q.D.; formal analysis, D.Z.; investigation, D.Z.; resources, D.Z.; writing—original draft preparation, Q.D.; writing—review and editing, Q.D.; visualization, D.Z.; supervision, D.Z. All authors have read and agreed to the published version of the manuscript.

Funding: This research was funded by Research Program supported by the 111 project (B16038), China.

Conflicts of Interest: The authors declare no conflict of interest.

References

1. Gil, L.; Otin, S.F.; Embid, J.M.; Gallardo, M.A.; Blanco, S.; Artal, M.; Velasco, I. Experimental setup to measure critical properties of pure and binary mixtures and their densities at different pressures and temperatures: Determination of the precision and uncertainty in the results. *J. Supercrit. Fluids* **2008**, *44*, 123–138. [[CrossRef](#)]
2. Li, M.; Zhu, H.; Guo, J.; Wang, K.; Tao, W. The development technology and applications of supercritical CO₂ power cycle in nuclear energy, solar energy and other energy industries. *Appl. Therm. Eng.* **2017**, *126*, 255–275. [[CrossRef](#)]
3. Zhao, H.; Deng, Q.; Huang, W.; Feng, Z. Thermodynamic and economic analysis and multi-objective optimization of supercritical CO₂ Brayton cycles. *J. Eng. Gas Turbines Power* **2016**, *138*, 1602. [[CrossRef](#)]
4. Park, S.; Kim, J.; Yoon, M.; Rhim, D.; Yeom, C. Thermodynamic and economic investigation of coal-fired power plant combined with various supercritical CO₂ Brayton power cycle. *Appl. Therm. Eng.* **2018**, *130*, 611–623. [[CrossRef](#)]
5. Turchi, C.; Ma, Z.; Neises, T.; Wagner, M. Thermodynamic study of advanced supercritical carbon dioxide power cycles for concentrating solar power systems. *J. Sol. Energy Eng.* **2013**, *135*, 1007. [[CrossRef](#)]
6. Xu, W.; Yang, J. Spiral-grooved gas face seal for steam turbine shroud tip leakage reduction: Performance and feasibility analysis. *Tribol. Int.* **2016**, *98*, 242–252. [[CrossRef](#)]
7. Doğu, Y.; Sertçakan, M.; Bahar, A.; Piskin, A.; Arican, E.; Kocagul, M. CFD Investigation of Labyrinth Seal Leakage Performance Depending on Mushroom Shaped Tooth Wear. In Proceedings of the ASME Turbo Expo: Turbine Technical Conference and Exposition, Montreal, QC, Canada, 15–19 June 2015; American Society of Mechanical Engineers: New York, NY, USA, 2015.
8. Zhang, L.; Zhu, H.; Liu, C.; Tong, F. Experimental and Numerical Investigation on Leakage Characteristic of Stepped Labyrinth Seal. In Proceedings of the ASME Turbo Expo: Turbomachinery Technical Conference

- and Exposition, Seoul, Korea, 13–17 June 2016; American Society of Mechanical Engineers: New York, NY, USA, 2016.
9. Wu, T.; San Andres, L. Gas labyrinth seals: On the effect of clearance and operating conditions on wall friction factors—A CFD investigation. *Tribol. Int.* **2019**, *131*, 363–376. [[CrossRef](#)]
 10. Wu, T.; San Andrés, L. Leakage and Dynamic Force Coefficients for Two Labyrinth Gas Seals: Teeth-on-Stator and Interlocking Teeth Configurations. A Computational Fluid Dynamics Approach to Their Performance. *J. Eng. Gas Turbines Power* **2019**, *141*, 042501. [[CrossRef](#)]
 11. Wróblewski, W.; Frączek, D.; Marugi, K. Leakage reduction by optimisation of the straight-through labyrinth seal with a honeycomb and alternative land configurations. *Int. J. Heat Mass Transfer* **2018**, *126*, 725–739. [[CrossRef](#)]
 12. Nayak, K.; Dutta, P. Numerical investigations for leakage and windage heating in straight-through labyrinth seals. *J. Eng. Gas Turbines Power* **2016**, *138*, 012507. [[CrossRef](#)]
 13. Desando, A.; Rapisarda, A.; Campagnoli, E.; Taurino, R. Numerical analysis of honeycomb labyrinth seals: Cell geometry and fin tip thickness impact on the discharge coefficient. In Proceedings of the ASME Turbo Expo: Turbine Technical Conference and Exposition, Montreal, QC, Canada, 15–19 June 2015; American Society of Mechanical Engineers: New York, NY, USA, 2015.
 14. Yan, X.; Dai, X.; Zhang, K.; Li, J.; He, K. Influence of hole-pattern stator on leakage performance of labyrinth seals. In Proceedings of the ASME Turbo Expo: Turbomachinery Technical Conference and Exposition, Oslo, Norway, 11–15 June 2018; American Society of Mechanical Engineers: New York, NY, USA, 2018.
 15. Zhang, W.; Yang, J.; Li, C.; Tian, Y. Comparison of leakage performance and fluid-induced force of turbine tip labyrinth seal and a new kind of radial annular seal. *Comput. Fluids* **2014**, *105*, 125–137. [[CrossRef](#)]
 16. Liu, Y.; Zhang, M.; Zhang, T.; Zhang, M.; He, Y. Effect of winglet-shroud tip with labyrinth seals on aerodynamic performance of a linear turbine cascade. *J. Fluids Eng.* **2016**, *138*, 071103. [[CrossRef](#)]
 17. Giboni, A.; Wolter, K.; Menter, J.; Pfost, H. Experimental and numerical investigation into the unsteady interaction of labyrinth seal leakage flow and main flow in a 1.5-stage axial turbine. In Proceedings of the ASME Turbo Expo: Power for Land, Sea, and Air, Vienna, Austria, 14–17 June 2004; American Society of Mechanical Engineers: New York, NY, USA, 2008; pp. 983–992.
 18. Fiedler, J.; Weber, A.; Bosco, A.; Engel, K.; Mare, F. Numerical simulation of the flow in the row labyrinth seal of an axial turbine using a low-Mach preconditioning technique. In Proceedings of the ASME Turbo Expo: Turbomachinery Technical Conference and Exposition, Seoul, Korea, 13–17 June 2016; American Society of Mechanical Engineers: New York, NY, USA, 2016.
 19. Kosowski, K.; Stepień, R. Reduction of pressure forces in turbine labyrinth seals. In Proceedings of the ASME Turbo Expo: Power for Land, Sea, and Air, Glasgow, UK, 14–18 June 2010; American Society of Mechanical Engineers: New York, NY, USA, 2010; pp. 2181–2197.
 20. Zou, Z.; Liu, J.; Zhang, W.; Wang, P. Shroud leakage flow models and a multi-dimensional coupling CFD (computational fluid dynamics) method for shrouded turbines. *Energy* **2016**, *103*, 410–429. [[CrossRef](#)]
 21. Biester, M.; Mueller, L.; Seume, J.; Guendogdu, Y. Time-resolved numerical investigation of the interaction of labyrinth seal leakage and main-flow in a 1.5-stage lp turbine. In Proceedings of the ASME 2011 Turbo Expo: Turbine Technical Conference and Exposition, Vancouver, BC, Canada, 6–10 June 2011; American Society of Mechanical Engineers: New York, NY, USA, 2012; pp. 1623–1632.
 22. Yuan, H.; Pidaparti, S.; Wolf, M.; Edlebeck, J.; Anderson, M. Numerical modeling of supercritical carbon dioxide flow in see-through labyrinth seals. *Nucl. Eng. Des.* **2015**, *293*, 436–446. [[CrossRef](#)]
 23. Kim, M.; Bae, S.; Son, S.; Oh, B.; Lee, J. Study of critical flow for supercritical CO₂ seal. *J. Heat Mass Transfer* **2019**, *138*, 85–95. [[CrossRef](#)]
 24. Kang, Y.; Huh, J.; Cho, J.; Shin, H.; Baik, Y. Design and performance assessments of a partial admission axial turbine using supercritical carbon dioxide. In Proceedings of the ASME Fluids Engineering Division Summer Meeting collocated with the ASME Heat Transfer Summer Conference and the ASME 14th International Conference on Nanochannels, Microchannels, and Minichannels, Washington, DC, USA, 10–14 July 2016; American Society of Mechanical Engineers: New York, NY, USA, 2016.
 25. Pugachev, A.; Kleinhans, U.; Gaszner, M. Prediction of rotordynamic coefficients for short labyrinth gas seals using computational fluid dynamics. *J. Eng. Gas Turbines Power* **2012**, *134*, 062501. [[CrossRef](#)]

26. McLinden, M. NIST thermodynamic and transport properties of refrigerants and refrigerant mixtures-REFPROP. In *NIST Standard Reference Database 23*; National Institute of Standards and Technology: Gaithersburg, MD, USA, 1998.
27. Zhou, A.; Song, J.; Li, X.; Ren, X.; Gu, C. Aerodynamic design and numerical analysis of a radial inflow turbine for the supercritical carbon dioxide Brayton cycle. *Appl. Therm. Eng.* **2018**, *132*, 245–255. [[CrossRef](#)]
28. Luo, D.; Liu, Y.; Sun, X.; Huang, D. The design and analysis of supercritical carbon dioxide centrifugal turbine. *Appl. Therm. Eng.* **2017**, *127*, 527–535. [[CrossRef](#)]



© 2020 by the authors. Licensee MDPI, Basel, Switzerland. This article is an open access article distributed under the terms and conditions of the Creative Commons Attribution (CC BY) license (<http://creativecommons.org/licenses/by/4.0/>).